Synthesis and Amyloid Binding Properties of Rhenium Complexes: Preliminary Progress Toward a Reagent for SPECT Imaging of Alzheimer's Disease Brain

Weiguo Zhen,[†,‡,⊥,▽] Hogyu Han,[‡,⊥,§] Magdalena Anguiano,[†,‡] Cynthia A. Lemere,[†] Cheon-Gyu Cho,[†,‡,∥] and Peter T. Lansbury, Jr.*[,†]

Center for Neurologic Diseases, Brigham and Women's Hospital and Harvard Medical School, Harvard Institutes of Medicine, Room 754, 77 Avenue Louis Pasteur, Boston, Massachusetts 02115, and Department of Chemistry, Massachusetts Institute of Technology, Cambridge, Massachusetts 02139

Received March 8, 1999

The definitive diagnosis of Alzheimer's disease (AD) requires the detection of amyloid plaques in postmortem brain. Although the amount of fibrillar amyloid roughly correlates with the severity of symptoms at the time of death, the temporal relationship between amyloid deposition, neuronal loss, and cognitive decline is unclear. To elucidate this relationship, a noninvasive, practical method for the quantitation of brain amyloid deposition is required. We describe herein the initial stages of a strategy to accomplish this goal by single photon computed tomographic imaging. The amyloid-binding dye Congo Red was modified to allow its conjugation to the monoamine-monoamide bis(thiol) ligand. This ligand complexes technetium(V) in its neutral oxo form. A biphenyl-containing building block was conjugated to the protected ligand, and the product was coupled to the relevant aromatic compounds. Rhenium oxo complexes, which are isosteric, but nonradioactive, analogues of the potential imaging agent technetium oxo complexes, were synthesized. These complexes bound to Aβ amyloid fibrils produced in vitro and stained amyloid plaques and vascular amyloid in AD brain sections.

Introduction

Alzheimer's disease (AD) is currently diagnosed based on the clinical observation of cognitive decline, coupled with the systematic elimination of other possible causes of those symptoms.[1,2] The confirmation of the clinical diagnosis of "probable AD" can only be made by examination of the postmortem brain.[1,3,4] The AD brain is characterized by a loss of neurons in regions of the brain responsible for learning and memory (e.g., hippocampus) and by the appearance, in these regions, of two distinct abnormal proteinaceous deposits: extracellular amyloid plaques, which are characteristic of AD, and intracellular neurofibrillary tangles (NFTs), which are found in other neurodegenerative disorders.[1−4] The amount of amyloid deposits roughly correlates with the severity of symptoms at the time of death;[5] although synaptic count, a more downstream marker, correlates more closely.

Amyloid plaques comprise dystrophic neurites and other altered astrocytes and microglia surrounding an insoluble fibrillar core. AD amyloid fibrils comprise a family of proteins known collectively as the amyloid β-proteins (Aβ), predominantly two variants: Aβ40 and Aβ42.[6] Aβ is derived from the ubiquitously expressed cell surface amyloid precursor protein (APP).[3,4,7] Several lines of circumstantial evidence suggest that Aβ amyloid fibril formation is an initiating event in the AD pathogenic cascade: (1) overexpression of APP is characteristic of Down syndrome, and early-onset AD is a virtual certainty in this population;[8,9] (2) missense mutations in APP cause early-onset AD;[3,7] (3) mutations in the presenilin proteins that also cause early-onset AD all increase the expression of the variant Aβ42 that is known to fibrillize more rapidly than Aβ40;[7,10−12] (4) the apoE variant encoded by the apoE4 allele, which confers susceptibility to late-onset AD, is more permissive of Aβ amyloid formation than the other apoE variants;[13−16] and (5) transgenic mice that overexpress mutant APP develop AD-like neuropathology.[17,18] While these facts strongly suggest that amyloid formation precedes neurodegeneration, a direct proof is lacking.

We sought to elucidate the relationship between amyloid formation and neurodegeneration by designing amyloid probes that could be used to measure brain amyloid noninvasively by single photon computed tomography (SPECT).[19−26] Three approaches to the SPECT imaging of amyloid fibrils, all involving protein probes, have been reported. The amyloid-associated protein serum amyloid P component (SAP), labeled with ^{123}I, accumulates at low levels in the cerebral cortex, possibly in vessel walls, of patients with cerebral amyloidosis.[19] Two other approaches have been discussed but have not been reduced to practice. Iodinated Aβ1−40, which binds AD amyloid plaque in tissue sections, can be transported across the blood−brain barrier (BBB) by conjugation to a protein that is actively transported.[25] In addition, antibodies to Aβ have been proposed to be useful imaging probes, although a method to deliver these probes across the BBB has not been described.[24] These approaches suffer from some or all of these disadvantages: (1) ^{123}I is not an ideal radioisotope for SPECT applications, since it must be generated in a

† Brigham and Women's Hospital and Harvard Medical School.
‡ Massachusetts Institute of Technology.
⊥ These two authors contributed equally to this work.
▽ Current address: Perkin-Elmer Biosystems, Foster City, CA 94404.
§ Current address: Department of Chemistry, Korea University, 1-Anamdong, Seoul 136-701, Korea.
∥ Current address: Department of Chemistry, Hangyang University, 17 Haengdang-Dong, Sungdong-Ku, Seoul 133-791, Korea.

10.1021/jm990103w CCC: $18.00
Published on Web 07/02/1999

Chart 1. Congo Red (**1**) and a Technetium Complex of Its Bipyridyl Analogue **2**

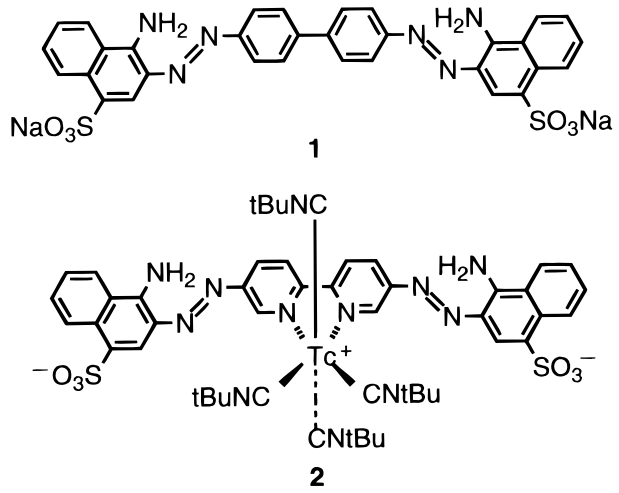

cyclotron; (2) proteins are susceptible to proteolysis; (3) most proteins do not cross the BBB; (4) proteins penetrate tissue poorly; and (5) proteins, especially antibodies, can be difficult to mass produce.

We chose to take a straightforward approach to the design of a low-molecular-weight, nonprotein amyloid probe by redesigning Congo Red (**1**, CR; Chart 1), a molecule that has been used for many decades to stain amyloid plaques in AD brain tissue sections. Congo Red stains amyloid in tissue to produce birefringent staining, indicative of long-range order of binding sites. Analysis of the fibril-binding properties of several analogues of CR established that the central biphenyl moiety could be modified at the 2 and 2′ positions without significantly diminishing the amyloid affinity.[22] Furthermore, introduction of a metal-binding bipyridyl unit and chelation of ^{99}Tc did not reduce amyloid affinity.[23] However, the resultant Tc(bipyridyl) complex **2** (Chart 1) has two disadvantages relevant to its use as an imaging agent. First, the mode of technetium complexation results in a positive charge on the metal, which may impede or prevent transport across the BBB.[21,27−31] Second, there is no simple way to make this complex in high yield and purity on a very small scale, a requirement for this probe to be useful clinically. To solve both of these problems, we sought to employ the monoamine-monoamide bis(thiol) (MAMA′) ligand, which chelates technetium(V) as a neutral oxo complex.[28,32−40] A compound comprising a Tc(MAMA′) oxo complex conjugated to a high-affinity ligand for the dopamine transporter crosses the BBB in a rhesus monkey and can be shown, by SPECT imaging, to accumulate in the striatum.[28,39,41,42] In addition, the Tc(MAMA′) complex is simple to prepare from readily available sources of ^{99m}Tc.[28,36,37,39,40] Finally, nonradioactive rhenium(MAMA′) oxo complexes can be simply prepared and used for biochemical studies that do not require radioactivity, since they are isosteric and isoelectronic with the Tc complexes.[33,36,37,40]

We report herein the synthesis of one technetium-99 oxo complex and two rhenium oxo complexes that are models of potential SPECT imaging agents for AD amyloid. The rhenium complexes bound to amyloid fibrils in vitro with comparable affinity to CR and similarly stained amyloid plaques in tissue sections from AD brain.

Results

Synthesis of the Biphenyl Linker, Triamine 5. Diazotization of 2-amino-4,4′-dinitrobiphenyl followed by nucleophilic aromatic substitution afforded the iodide **3** (Scheme 1), which was subsequently converted to the nitrile **4**. Attempts to produce **4** via the bromide analogue of **3**[42] were less successful, since formation of the bromide and its conversion to **4** proceeded in significantly lower yields. Hydrogenation of the nitro groups followed by reduction of the nitrile provided the triamine **5** in 61% overall yield from the starting monoamine. Ten grams of triamine **5** have been produced in comparable yield by this reaction sequence.

Conjugation of the MAMA′ Ligand. The MAMA′ ligand **6**[36,37,40,43] was alkylated with β-bromopropionate to produce ester **7** in good yield (Scheme 2). Hydrolysis of the ester, followed by treatment with dicyclohexylcarbodiimide (DCC), afforded the DCC ester, which was converted to the *N*-hydroxysuccinimide (NHS) ester. The NHS ester was added, without purification, to a solution of 1 equiv of triamine **5** to afford compound **8** in ca. 78% yield from **6**. This strategy compares favorably with the alternative method of MAMA′ ligation by alkylation, in which the primary alkyl halide intermediate is susceptible to elimination.[28,39]

Compound **8** was diazotized by a standard method and separately coupled to two activated aromatic compounds (Scheme 3). The optimal conditions for these two couplings were not identical, due to the different solubilities and pK_a's of the aromatic compounds. Treatment of diazotized **8** with 4-amino-1-naphthalenesulfonic acid, as sodium salt, provided the CR analogue **9** in 60% yield. Alternatively, treatment with 1-hydroxy-2-naphthoic acid, as sodium salt, afforded compound **11** in 60% yield. This compound is a naphthyl congener of chrysamine G (CG), a dye that has affinity for amyloid fibrils comparable to that of CR.[20,21,23] Coupling to *o*-hydroxybenzoic acid, to produce the CG analogue, was unsuccessful. Since the hydroxy group ortho to the carboxylic acid moiety present in **11** (and **14**) will delocalize its effective charge of the carboxylate via intramolecular hydrogen bonding, these compounds should be less polar than the CR analogues and may be more likely to cross the BBB (see below). The CR analogue **9** was deprotected with silver nitrate[23,44−48] and treated, without purification, with ammonium pertechnate (^{99}Tc), to afford, after purification, the technetium-99 complex **10** in 88% yield. This procedure must be modified for incorporation of technetium-99m; hence compound **11** was not converted to the corresponding technetium-99 complex. In addition, the isosteric rhenium oxo complexes were synthesized by an alternative route.

Synthesis of the Rhenium Oxo Complexes. The direct conversion of compounds **9** and **11** to the analogous rhenium complexes was not possible because the conditions for Re complexation reduced the diazo bonds in the product. Therefore, complexation of Re to **8** was accomplished prior to diazo coupling. The major product **12** was a single isomer, presumed to be *syn* with respect to the Re oxo bond and the linker because: (1) all known

Scheme 1. Production of Triamine **5**[a]

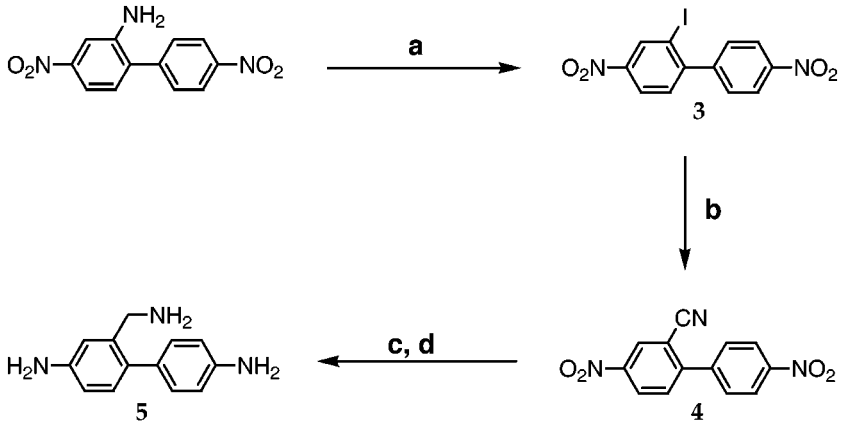

[a] Reagents and conditions: (a) H_2SO_4/KI, $NaNO_2$, 5 °C; (b) CuCN, DMSO, Δ; (c) Pd/C, MeOH, 25 °C; (d) $LiAlH_4$, THF, Δ.

Scheme 2. Production of Compound **8**[a]

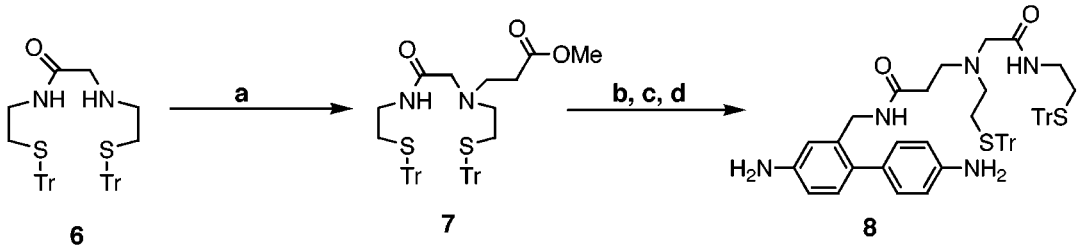

[a] Reagents and conditions: (a) methyl 3-bromopropionate, $KHCO_3/K_2CO_3$, CH_3CN, Δ; (b) LiOH, 1:1 MeOH/H_2O, 25 °C; (c) NHS, DCC, THF, 25 °C; (d) **5**/THF, 25 °C.

examples of Re complexes of this type are predominantly *syn*,[28,40] and (2) the diagnostic ^{1}H NMR resonances of the protons α to the tertiary amine in the *anti* complex linker are not seen in the ^{1}H NMR spectrum of **12**.[28,49] The infrared absorption frequency of the Re−oxo bond in **12** was not informative in this regard, since the experimental absorption of 967 cm^{-1} is midway between published absorptions of 955 cm^{-1} for a model *syn* complex and 980 cm^{-1} for a model *anti* complex.[40] Rhenium complex **12** (Scheme 4) was successfully diazotized and coupled to both 4-amino-1-naphthalenesulfonic acid and 1-hydroxy-2-naphthoic acid, both as sodium salt, in moderate yield, to afford the Re complexes **13** and **14**, respectively.

The Rhenium Oxo Complex 14 Is Relatively Hydrophobic. The partitioning of a compound between aqueous buffer and octanol roughly correlates with its ability to cross the BBB by passive transport; that is, compounds that prefer octanol are more likely to cross.[20,30,50] This property is expressed as the *P* value, where *P* is the concentration in octanol phase/concentration in aqueous phase. It has been proposed that a *P* value between 7.8 and 316 (log *P* between 0.9 and 2.5) is optimal for BBB crossing.[30] We measured a *P* value of 0.16 ± 0.02 for CR. This value compares to a *P* value of 0.323 ± 0.015 for CR using a different aqueous buffer (the same paper reports a *P* value of 3.69 ± 0.21 for CG).[20] The Re complex based on CR, **13**, had a *P* value of 0.12 ± 0.04, comparable to that of CR. Compound **14**, loosely based on the CG structure, had a *P* value of 4.6 ± 0.9 (log $P = 0.70$), indicative of its significantly greater hydrophobicity. It is expected that the ^{99m}Tc analogues of **13** and **14** will have similar polarities as the Re complexes.

The Rhenium Oxo Complexes 13 and 14 Have Comparable Affinity for Aβ40 Amyloid Fibrils as Congo Red. CR, **13**, and **14** showed saturable binding to amyloid fibrils formed in vitro from synthetic Aβ40.[23] Since compound **14** is insoluble at high salt, binding studies were done at pH 7.4, in 10 mM phosphate buffer, with and without an added 100 mM NaCl. The intrinsic affinity of CR for Aβ40 fibrils was insensitive to salt; K_d (apparent dissociation constant) was measured to be 1.5 ± 0.005 μM at 110 mM salt and 1.1 ± 0.4 μM at 10 mM salt (Figure 1). However, the stoichiometry of binding site saturation *was* salt-sensitive; more sites on the Aβ40 fibril were available at high salt (B_{max} is 2.6 ± 0.14 mol of CR bound/mol of Aβ40 vs 0.60 ± 0.05 at low salt). The salt effect suggests that fibril−CR interactions are not predominantly ionic in nature (in contrast to one model for binding[20]), but interactions between bound dye molecules may be. Thus ionic shielding of sulfonate groups projecting away from the fibril surface may allow closer approach of like-charged dye molecules and a higher stoichiometry of binding. The rhenium complex **13** bound with comparable affinity as CR at high salt ($K_d = 1.1 \pm 0.2$ μM), but with lower stoichiometry ($B_{max} = 0.44 \pm 0.07$). In contrast, at low salt, compound **14** bound slightly more avidly to Aβ40 amyloid fibrils than did CR ($K_d = 0.83 \pm 0.04$ μM), with a higher stoichiometry ($B_{max} = 1.4 \pm 0.05$).

Staining of AD Brain Tissue with Rhenium Oxo Complexes 13 and 14. Rhenium complexes **13** and **14** were utilized to stain AD brain sections, following a standard CR staining protocol for paraffin sections (see Experimental Section). Serial sections were stained with CR, Re complex **13**, and Re complex **14**. Each complex produced birefringence, yellow/green in the case of CR

Scheme 3. Production of Bistrityl Precursors and Technetium Complex **10**[a]

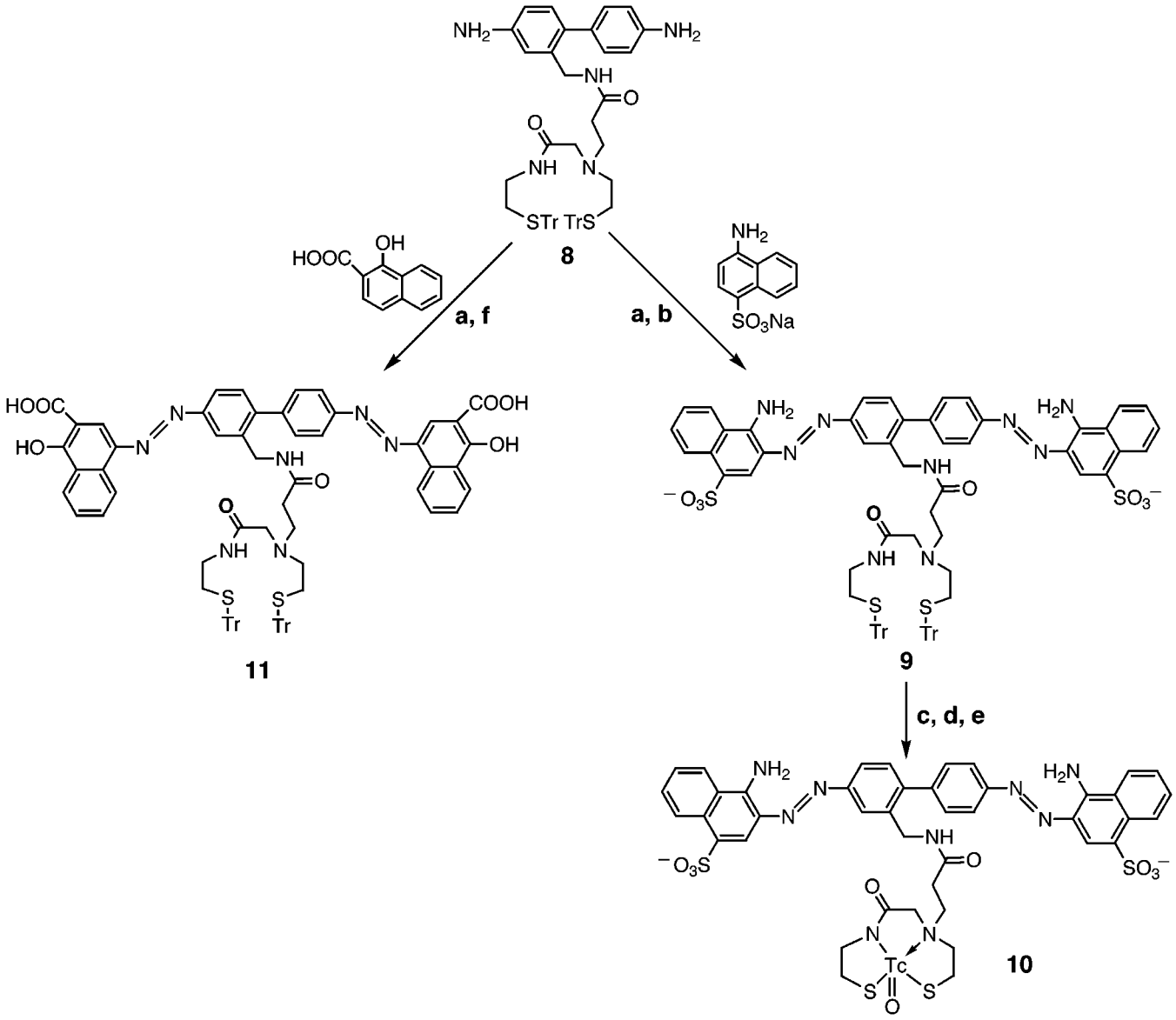

[a] Reagents and conditions: (a) $NaNO_2$, THF/H_2O/HCl, 5 °C, 2 min; (b) 4-amino-1-naphthalenesulfonic acid sodium salt, NaOAc/Na_2CO_3/THF, 5 °C; (c) $AgNO_3$, 1:1 MeOH/H_2O, 25 °C; (d) DTT, 1:1 THF/H_2O, then Na_2CO_3, 25 °C; (e) NH_4TcO_4, NaOH/EtOH, 75 °C; (f) 1-hydroxy-2-naphthoic acid, Na_2CO_3/THF, 5 °C.

and **13** and yellow/white in the case of **14**, indicative of ordered long-range binding (Figure 2). However, a 2.5-fold higher concentration of **14** had to be utilized in order to observe birefringent staining over background. This may simply be a reflection of the shifted absorption of the induced birefringence, which makes it difficult to distinguish from background. Fibrillar Aβ amyloids, both in blood vessel walls and in plaques (plaques were located by immunostaining with an anti-Aβ antibody), were detected by each compound. This pattern of staining (i.e., lesion specificity) was consistent for all three dyes; however, the intensity of birefringence for CR and **13** was brighter than for **14**. For all three compounds, vascular amyloid was labeled more intensely than plaque amyloid, possibly reflecting a greater density of Aβ fibrils in vascular amyloid (Figure 2).

Discussion

The quantitation of brain amyloid by a simple, inexpensive, and noninvasive imaging method could have major repercussions for the understanding of the pathogenesis of AD and also for its diagnosis and treatment. First, fibrillar amyloid quantitation would allow for a confirmation of the clinical diagnosis of "probable AD", which is based on the observation of dementia and the systematic elimination of other possible causes. Second, it may allow for the detection of early disease in individuals who have not yet developed symptoms. These individuals, who could be targeted for imaging based on their "AD susceptibility profile" (e.g., apoE genotype, family history, incidence of head trauma, etc.), are likely to be more easily treated than symptomatic individuals, who have extensive neurodegeneration. Finally, such a method would be valuable both for clinical trials, to monitor the effect of treatment with amyloid inhibitors, and eventually for monitoring the dose of such a drug in a clinical setting.[51]

SPECT imaging is the ideal method for the quantitation of brain amyloid, since presence and amount of fibrillar amyloid, not its high-resolution anatomical

Scheme 4. Production of Rhenium Complexes **13** and **14**[a]

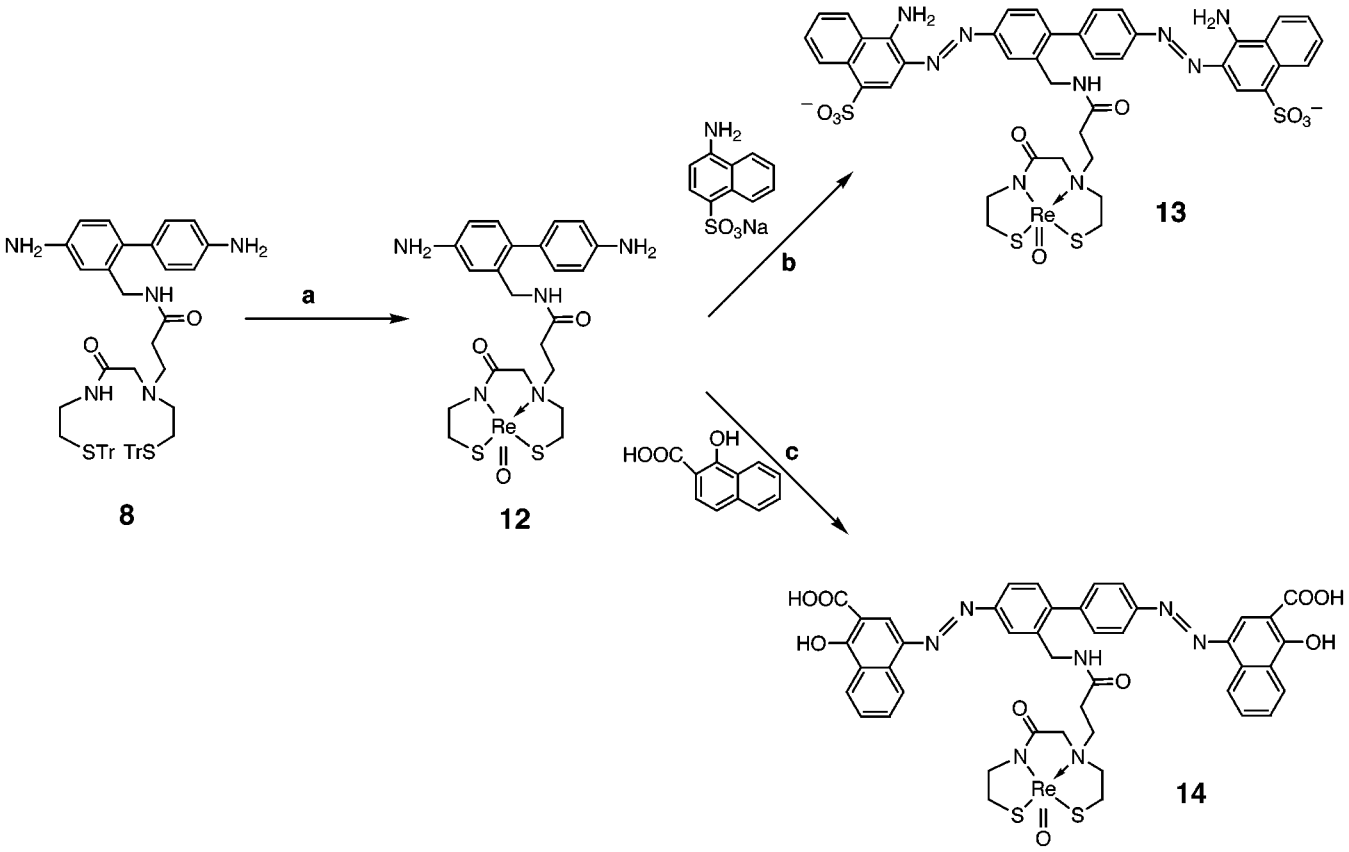

[a] Reagents and conditions: (a) MeOH/THF/HCl, $SnCl_2/NaReO_4$, Δ; (b) 4-amino-1-naphthalenesulfonic acid sodium salt, NaOAc/Na_2CO_3/THF, 5 °C; (c) 1-hydroxy-2-naphthoic acid, Na_2CO_3/THF, 5 °C.

localization, is the critical issue. An ideal amyloid SPECT probe would incorporate ^{99m}Tc, the optimal radioisotope for SPECT.[39,41] In addition, such a probe would: (1) utilize a practical method of technetium complexation such that the complex could be prepared in a radiopharmacy immediately prior to its use; (2) be easily accessible in large quantities at high purity; (3) demonstrate a high practical affinity for amyloid, that is, be able to distinguish AD tissue from age-matched normal brain that typically contains little or no fibrillar amyloid; (4) be physiologically stable; (5) cross the BBB in sufficient quantities to allow realization of point (3); and (6) be nontoxic. This manuscript addresses points (1) and (2). The amyloid probes described herein utilize a practical method of Tc complexation identical to that of the brain imaging agent Technepine.[39] In addition, the probe precursors can be prepared in large quantities by a simple sequence of reactions. The practical issues of ^{99m}Tc incorporation, which should ideally be accomplished in a simple final step at the imaging site (this rules out the route used herein for production of Re complexes **13** and **14**), remain to be solved.

Regarding point (3), the in vitro affinity of probes **13** and **14** for Aβ40 amyloid fibrils is comparable to that of CR and CG, in the high-nanomolar/low-micromolar range.[20,21,23] The relationship between this value and the effective in vivo affinity is complex. The latter involves, in addition to the intrinsic affinity, the stoichiometry of binding (B_{max} herein), the deliverable local concentration, the number of binding sites in the target tissue, and the kinetics of BBB crossing in both directions. Practical affinity can therefore only be optimized by iterative experimentation in a live organism. Nevertheless, in vitro affinity of these probes can be optimized by screening of analogue libraries. The synthetic route outlined above is adaptable to a parallel synthesis mode, whereby libraries of analogues, with different aromatic termini flanking the biphenyl core, for example, could be produced and screened for tight binding and specificity. The rhenium complexes **13** and **14** stain AD brain sections in a manner similar to CR. It remains to be demonstrated that the specific lesion binding that is selectively visualized by birefringence (Figure 2) represents a sufficient portion of the total binding (i.e., birefringent + nonspecific) such that a difference between normal brain and AD brain can be measured by SPECT. It is encouraging that the analogous azo dye [^{14}C]CG binds to AD brain tissue in significantly greater amount than to normal brain tissue.[21]

Points (4), (5), and (6) are not addressed in these studies. However, there are published reports regarding analogous compounds that are relevant to each point. These complexes, in contrast to protein-imaging agents,[19,24,25] are expected to be physiologically stable. The reductive cleavage of diazo bonds in analogous dyes, including CR, proceeds at low levels in biological media.[52] However, [^{14}C]CG, recovered from mouse brain and liver 1 h after intravenous injection, was >95% radiochemically pure as judged by HPLC.[21] This result suggests that the physiological stability of these complexes may be adequate for SPECT studies.

The ability of these complexes to cross the BBB in quantities sufficient to realize point (3) is difficult to

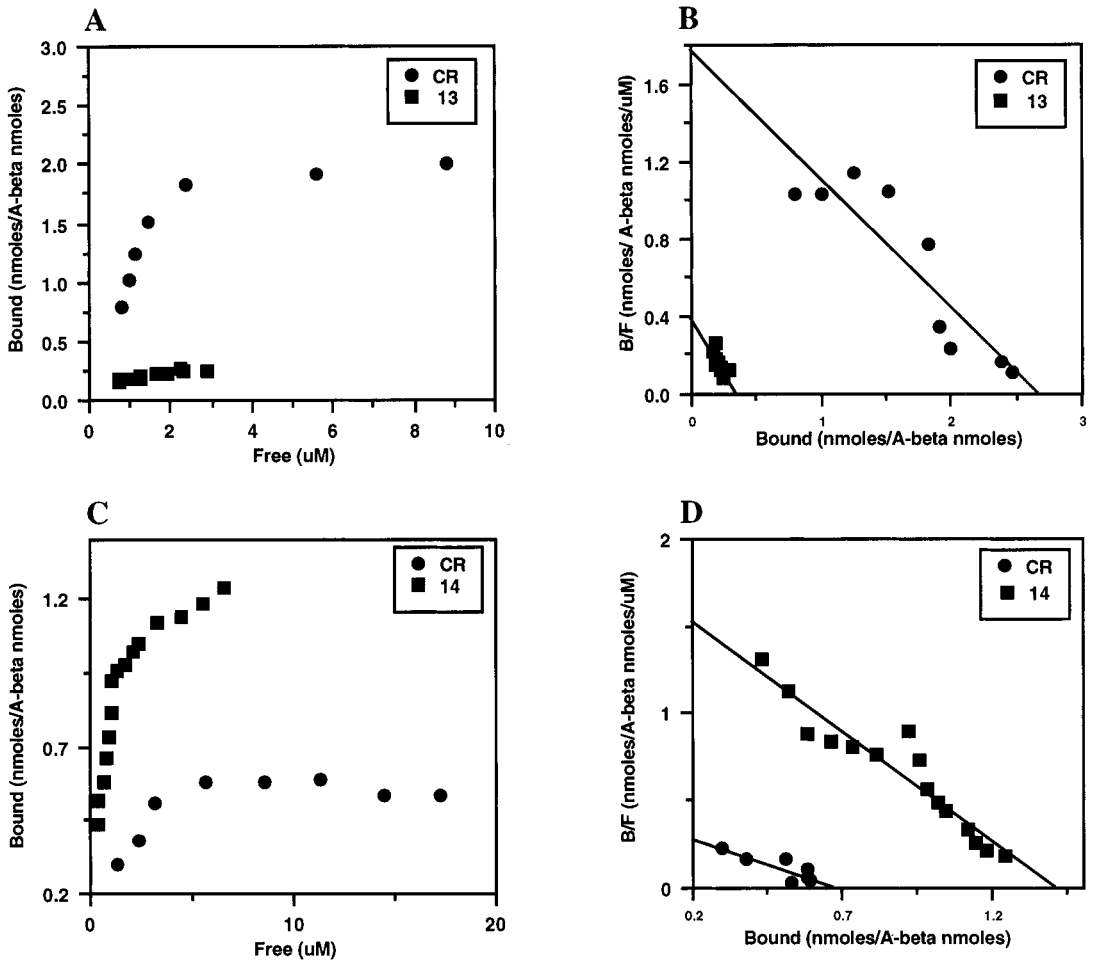

Figure 1. Standard binding curves are shown in the left column, with Scatchard double-reciprocal plots in the right column. Panels A and B show a comparison of CR and compound **13** at high salt (110 mM, see text). Panels C and D show a comparison of CR and compound **14** at low salt (10 mM).

predict. The ability of a compound to cross the BBB is correlated to its partition coefficient between octanol and aqueous buffer (*P* value).[30,42,50] However, it must be emphasized that this correlation is not linear, and these in vitro measurements cannot accurately predict the outcome of an in vivo study. The Re complex **14** has a *P* value of 4.6, which is very close to the optimal *P* values recommended for brain imaging.[30] Low-molecular-weight compounds cross the BBB more efficiently; the BBB-crossing ability seems to correlate inversely with the square route of the MW,[50] at least for compounds under 600 Da. There have been few studies of compounds in the MW range of these complexes (the Tc analogue of **14** has a MW of ca. 970), although peptide analogues with a MW over 1000 Da have been shown to cross.[19,25] By way of comparison, compounds with similar *P* values to that of **14** have been shown to cross the BBB at levels that may be sufficient for SPECT imaging (e.g., CG: $P = 3.7$, MW = 482[21]). Furthermore, several neutral Tc oxo complexes that were designed to label the dopamine transporter have been show to effectively cross the BBB and label the striatum in rhesus monkeys (Technepine: MW = 608, *P* is unreported[28,32]) and in humans (TRODAT: MW = 520, $P = 227$[40,41]). Although **10** is not likely to efficiently cross the BBB, it may be suitable for SPECT detection of systemic amyloid in patients suffering from systemic amyloid diseases such as B-cell myeloma or familial amyloidotic polyneuropathy.[53] In these populations, there is a clinical need to identify sites of amyloid deposition.

Finally, the toxicity of the technetium complexes discussed herein in the concentration range utilized for SPECT imaging is unlikely to be significant. Typical doses for SPECT imaging in humans are in the range of 10 μg/kg.[40] The LD_{50} of CR is reported to be 190 mg/kg in rats.[27] It has been reported that CG has no behavioral or toxic effects in mice for periods up to 72 h at doses of 100 mg/kg.[21] Finally CR is negative in the standard Ames test.[52]

In conclusion, the ^{99m}Tc analogues of **13** and, especially, **14** have the potential to be useful in imaging amyloid in AD brain. The synthetic challenges posed by practical issues surrounding Tc-99m complexation remain to be solved. In addition, in vivo studies are required in order to determine whether any of these probes cross the BBB in adequate concentrations and whether the ratio of specific to nonspecific binding allows the distinction of AD brain tissue from brain tissue of an age-matched, cognitively normal individual. However, the chemistry reported herein provides a critical first step toward this important goal.

Experimental Section

General. ^{1}H NMR spectra were recorded using a Varian XL-300 NMR spectrometer (300 MHz). Chemical shifts are

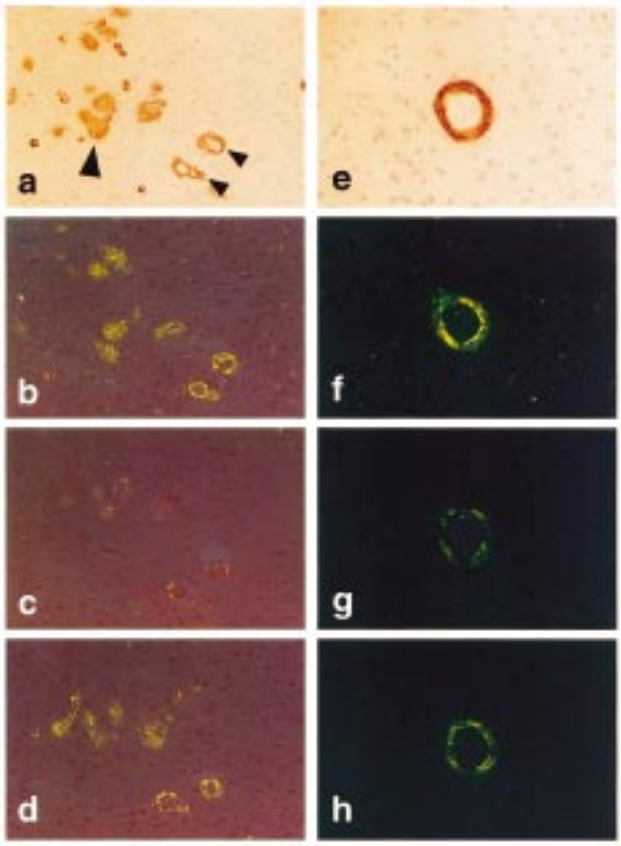

Figure 2. Staining of serial occipital sections from the brain of a 69-year-old AD patient with Aβ antibody (top row), CR (**1**) (second row), and rhenium complexes **14** (third row) and **13** (fourth row). a−d: Amyloid plaques (large arrowhead) and blood vessel walls (small arrowheads) in adjacent sections by each staining method (a, Aβ antibody R1282; b, CR (**1**); c, **14**; d, **13**). The horizontal and vertical axes in a−d represent 700 and 470 μm, respectively. e−h: Amyloid in the wall of a blood vessel in adjacent sections of occipital cortex of the same patient (e, R1282; f, **1**; g, **14**; h, **13**). The horizontal and vertical axes in e−h represent 350 and 235 μm, respectively. (Figure was reduced to 55% of original for reproduction.)

reported in parts per million downfield from tetramethylsilane, and coupling constants are in hertz (Hz). Mass spectra were recorded using fast atom bombardment (FAB) techniques (by Andrew Rhomberg of the MIT Mass Spectrometry Facility; supported by NIH Grant RR00317 to K. Biemann) or matrix-assisted laser desorption ionization (MALDI) mass spectrometry by Quality Controlled Biochemicals, Inc. (Hopkinton, MA). High-resolution mass spectra were measured at the MIT Department of Chemistry Spectroscopy Laboratory under either electron impact (EI) or FAB ionization conditions. Several compounds, notably **10** and **14**, did not produce parent ions under EI or FAB conditions; therefore, these were analyzed by a low-resolution MALDI technique. Preparative HPLC was performed on a Waters Prep LC 4000 system using a C_{18} reversed-phase column (22 × 250 mm, 15−20-μm particle size, TP silica; Vydac, Southboro, MA) with H_2O and MeOH as eluents at a flow rate of 15 mL/min. UV spectra were measured on a Hewlett-Packard 8452A diode array spectrophotometer. Flash chromatography was carried out using silica gel 60 (230−400; mesh EM Science). Thin-layer chromatography (TLC) was performed on silica gel 60 F_{254} precoated plates (250 μm; EM Science). All chemicals for synthesis were purchased from Aldrich unless otherwise specified. CR was purchased from Fluka and purified using preparative HPLC before use. All compounds reported herein were judged to be > 95% pure by TLC, HPLC, and ^{1}H NMR. Therefore, recrystallization for the sole purpose of melting point determination was not attempted.

2-Iodo-4,4′-dinitrobiphenyl, 3. To a 500-mL three-neck round-bottom flask charged with 15.6 g (60.3 mmol) of 2-amino-4,4′-dinitrobiphenyl was added 100 mL of concentrated sulfuric acid. After the mixture became homogeneous, the reaction was cooled to 0 °C. In a separate 100-mL flask containing 5.60 g (81.2 mmol) of sodium nitrite was slowly added 50 mL of sulfuric acid over 30 min at 5 °C. The resultant solution was then dropwise added to the amine solution with cooling. Manual agitation of the reaction mixture was necessary. Next, 150 mL of 85% phosphoric acid was added over 1 h via an addition funnel, during which time the temperature of the reaction mixture was maintained below 10 °C. The mixture was agitated periodically to ensure homogeneity. Conversion to the diazonium salt was monitored by adding a drop of the reaction mixture to 20 mL of water. When this solution turned light-yellow and no insoluble material was formed, the reaction was complete. The reaction mixture was then allowed to warm to room temperature over 2−3 h and added to 1000 mL of ice water with stirring. After 30 min, excess urea (12.0 g) was slowly added to consume excess nitrous acid, and the reaction mixture was stirred for 30 min. To this mixture was added an aqueous solution of potassium iodide (22.68 g in 150 mL, 129.4 mmol). The reaction mixture was then heated to 70 °C. The reaction mixture was extracted with CH_2Cl_2, dried over $MgSO_4$, and concentrated. The crude product was purified by silica gel chromatography (1:1 hexane:CH_2Cl_2) to afford the dinitroiodide product **3** (19.66 g, 53.72 mmol, 89% yield) as a light-yellow solid. ^{1}H NMR ($CDCl_3$): δ 8.82 (d, J = 2.1 Hz, 1H), 8.35 (d, J = 8.7 Hz, 2H), 8.30 (dd, J = 2.1, 8.8 Hz, 1H), 7.55 (d, J = 8.7 Hz, 2H), 7.48 (d, J = 8.4 Hz, 1H). ^{13}C NMR ($CDCl_3$): δ 150.4, 148.1, 147.8, 147.5, 134.50, 129.9, 128.2, 124.2, 123.6, 123.2. HRMS: EI parent ion, $C_{12}H_7N_2O_4I$, 369.9455; calcd, 369.9450. Anal. (exptl. (calcd)): C 39.07 (38.94), H 1.90 (1.91), N 7.54 (7.57).

2-Cyano-4,4′-dinitrobiphenyl, 4. A solution of the iodide **3** (10.0 g, 27.3 mmol) and CuCN (3.30 g, 36.8 mmol) in 60 mL of anhydrous dimethyl sulfoxide was heated (180 °C) under an argon atmosphere. After 2 h, the reaction mixture was added to a solution of aqueous ammonium chloride (200 mL) at 0 °C and filtered through a Buchner funnel. The insoluble product was partitioned into methylene chloride and water. The separated organic layer was dried over $MgSO_4$ and concentrated. The crude product was purified by silica gel chromatography (1:1 hexane:CH_2Cl_2 to 30%:69%:1% hexane:CH_2Cl_2:MeOH) to afford the nitrile **4** (6.60 g, 24.5 mmol, 90% from **3**) as a light-yellow solid. ^{1}H NMR ($CDCl_3$): δ 8.69 (d, J = 2.4 Hz, 1H), 8.56 (dd, J = 8.4, 2.4 Hz, 1H), 8.42 (d, J = 8.4 Hz, 2H), 7.78 (dd, J = 8.7, 1.8 Hz, 3H). ^{13}C NMR ($CDCl_3$): δ 148.7, 148.5, 147.5, 141.9, 131.3, 129.8, 128.9, 127.6, 124.9, 115.8, 113.0. HRMS: EI, $C_{13}H_7N_3O_4$, 269.0435; calcd, 269.0436. Anal. (exptl (calcd)): C 58.06 (57.98), H 2.58 (2.62), N 15.58 (15.61).

Triamine 5. A solution of nitrile **4** (3.0 g, 11 mmol) in methanol (150 mL) was shaken with 10% Pd on C (500 mg) under H_2 (55 psi) for 24 h using a Parr apparatus. The reaction mixture was filtered through Celite and concentrated to afford the diaminonitrile as a yellow solid (2.2 g, 11 mmol, 96%), R_f = 0.54 (7:93 MeOH:CH_2Cl_2). The crude product was dissolved in tetrahydrofuran (5 mL) and added dropwise to a suspension of $LiAlH_4$ (3.0 g, 79 mmol) in THF (90.0 mL), and the reaction mixture was heated at reflux under argon. After 8 h, the reaction mixture was cooled to room temperature and quenched by sequential addition of H_2O and 5% NaOH. The mixture was filtered to remove insoluble aluminum salts, and the filtrate was extracted with CH_2Cl_2, dried over potassium carbonate, filtered, and concentrated in vacuo to give the triamine **5** as a tan oil. The oil was further purified by redissolving in 200 mL of pH 1−2 water and extracted with CH_2Cl_2. The acidic aqueous solution was adjusted to pH 10−11 and exhaustively extracted with CH_2Cl_2 to give a light-yellow solid after evaporation (1.7 g, 8.1 mmol, 76% from **4**). ^{1}H NMR (DMSO-d_6): δ 6.97 (d, J = 8.3 Hz, 2H), 6.81 (d, J = 8.1 Hz, 1H), 6.73 (d, J = 1.8 Hz, 1H), 6.60 (d, J = 8.2 Hz, 2H), 6.47 (dd, J = 8.1, 2.2 Hz, 1H), 4.94 (bs, 4H), 4.20 (bs, 2H), 3.57 (bs, 2H). ^{13}C NMR

(DMSO-d_6): δ 147.6, 146.2, 132.8, 132.4, 132.0, 131.0, 127.8, 116.3, 116.0, 115.2, 67.1. MALDI MS for $C_{13}H_{15}N_3$ $[M + H]^+$: 213. HRMS: EI, 213.1254; calcd, 213.1265.

Compound 7. To a solution of MAMA′[36,37,40] (**6**; 5.36 g, 7.92 mmol) in acetonitrile (150 mL) were added methyl 3-bromopropionate (4.0 mL, 58 mmol), $KHCO_3$ (500 mg), and K_2CO_3 (500 mg). The reaction mixture was refluxed under argon at 80 °C for 12 h. After cooling to room temperature and filtering, the solution was concentrated. The crude product was purified by flash chromatography (hexane, then 1:3 ethyl acetate/hexane) to give compound **7** as a pale-yellow solid (3.9 g, 5.2 mmol, 65% from **6**; 87% based on recovered starting material), $R_f = 0.35$ (1:3 EtOAc:hexane). ^{1}H NMR ($CDCl_3$): δ 7.39 (t, J = 7.2 Hz, 12H), 7.17−7.26 (m, 18H), 3.53 (s, 3H), 3.05 (q, J = 7.0, 12 Hz, 2H), 2.85 (s, 2H), 2.60 (t, J = 7.0 Hz, 2H), 2.26−2.40 (m, 8H). ^{13}C NMR ($CDCl_3$): δ 172.3, 170.5, 144.7, 144.6, 129.5, 127.8, 126.7, 126.6, 66.8, 66.6, 58.2, 53.3, 51.6, 49.8, 37.9, 31.9, 31.7, 29.6. MALDI MS for $C_{48}H_{48}N_2O_3S_2Na$ $[M + Na]^+$: 786.28; calcd, 787.30. Anal. (exptl (calcd)): C 75.03 (75.36), H 6.64 (6.33), N 3.66 (3.66).

Compound 8. To a solution of **7** (3.1 g, 4.0 mmol) in MeOH (30 mL), H_2O (15 mL), and THF (30 mL) was added LiOH·H_2O (336 mg, 8.00 mmol). The resulting solution was stirred for 3 h at room temperature. Organic solvent was removed in vacuo, and the resultant aqueous solution was acidified to pH 4 with 10% HCl and extracted with ethyl acetate. The combined ethyl acetate fractions were dried over $MgSO_4$ and evaporated to give the acid as a white solid (3.0 g, $R_f = 0.71$, 7:1:92 MeOH:acetic acid:CH_2Cl_2). ^{1}H NMR (DMSO-d_6): δ 7.67 (t, J = 5.8 Hz, 1H), 7.31−7.18 (m, 30H), 2.95 (q, J = 6.7 Hz, 2H), 2.79 (s, 2H), 2.51−2.46 (m, 2H), 2.30−2.16 (m, 8H).

To a solution of the crude acid (3.0 g, 4.0 mmol) and *N*-hydroxysuccinimide (460 mg, 4.00 mmol) in THF (60 mL) was added 1,3-dicyclohexylcarbodiimide (860 mg, 2.00 mmol) in THF (20 mL). After stirring at room temperature for 2 h, the solution was filtered into a flask containing the triamine **5** (810 mg, 3.80 mmol) in THF (20 mL). After 2 h at room temperature, the reaction mixture was concentrated and the crude product was purified by flash chromatography (CH_2Cl_2, then 3:97 MeOH:CH_2Cl_2) to give compound **8** as a yellow solid (3.5 g, 3.6 mmol, 90% from **7**, $R_f = 0.49$, 7:1:92 MeOH:acetic acid:CH_2Cl_2). ^{1}H NMR (DMSO-d_6): δ 8.09 (t, J = 5.0 Hz, 1H), 7.71 (t, J = 5.4 Hz, 1H), 7.19−7.35 (m, 30H), 6.89 (d, J = 8.4 Hz, 2H), 6.82 (d, J = 8.7 Hz, 1H), 6.55 (d, J = 8.3 Hz, 2H), 6.47−6.49 (m, 2H), 4.99 (bs, 2H), 4.95 (bs, 2H), 4.04 (d, J = 6.4 Hz, 2H), 2.91−2.95 (m, 2H), 2.76 (s, 2H), 2.31−2.35 (m, 2H), 2.13−2.22 (m, 8H). ^{13}C NMR ($CDCl_3$): δ 170.8, 170.6, 145.6, 145.2, 144.7, 136.2, 131.8, 131.3, 130.9, 130.1, 129.5, 127.9, 126.7, 126.6, 114.9, 114.2, 66.9, 66.7, 58.0, 53.5, 50.2, 49.1, 41.7, 38.0, 33.9, 29.5. MALDI MS for $C_{60}H_{59}N_5O_2S_2Na$ $[M + Na]^+$: 968.01; calcd, 968.40. HRMS FAB $(M + H)^+$: 946.4182; calcd, 946.4188.

Compound 9. To a solution of **8** (50 mg, 0.053 mmol) in THF (5 mL), H_2O (2 mL), and 10% HCl (140 μL) at 5 °C was added a solution of $NaNO_2$ (8.0 mg, 0.12 mmol) in H_2O (40 μL). After stirring at 5 °C for 2 min, the resulting yellow solution was added dropwise to a solution of 4-amino-1-naphthalenesulfonic acid sodium salt (61 mg, 0.25 mmol), sodium acetate trihydrate (108 mg, 0.790 mmol), and Na_2CO_3 (10 mg, 0.094 mmol) in H_2O (1 mL) at 5 °C. A distinct color change from yellow to red was immediately observed. After the mixture stirred at 5 °C for 3 min, THF (1 mL) was added. After 1 h at 5 °C the mixture was concentrated, and the crude product was purified by flash chromatography (CH_2Cl_2, then 1:9, 3:7 MeOH:CH_2Cl_2) followed by preparative HPLC (0−5 min 10% MeOH, 5−20 min 10−100% MeOH gradient, 20−25 min 100% MeOH, R_v = 285−345 mL) to afford **9** as a red solid (45 mg, 0. 032 mmol, 60% from **8**, R_f = 0.29, 25:75 MeOH:CH_2Cl_2). UV (10 mM Na_2HPO_4, pH 7.4): λ_{max} 486 nm ($\epsilon = 2.90 \times 10^4$ cm^{-1}·M^{-1}), 322 nm ($\epsilon = 3.00 \times 10^4$ cm^{-1}·M^{-1}). ^{1}H NMR (CD_3OD): δ 8.81 (d, J = 8.1 Hz, 2H), 8.65 (d, J = 3.0 Hz, 1H), 8.29 (d, J = 7.9 Hz, 1H), 8.28 (d, J = 7.8 Hz, 1H), 7.96 (d, J = 2.0 Hz, 1H), 7.91 (d, J = 8.1 Hz, 3H), 7.66 (t, J = 7.9 Hz, 2H), 7.53 (t, J = 8.4 Hz, 4H), 7.46 (d, J = 7.5 Hz, 1H), 7.30−7.25 (m, 12H), 7.16−7.07 (m, 18H), 4.48 (s, 2H), 2.97 (t, J = 6.8 Hz, 2H), 2.86 (s, 2H), 2.62 (t, J = 5.9 Hz, 2H), 2.34−2.25 (m, 8H). ^{13}C NMR ($CDCl_3$): δ 174.1, 173.4, 159.0, 153.9, 153.5, 146.3, 146.1, 145.8, 143.1, 142.8, 138.0, 132.4, 132.1, 131.1, 130.6, 130.4, 130.3, 129.9, 128.9, 128.4, 127.7, 126.5, 126.0, 124.5, 124.4, 124.1, 123.5, 123.2, 68.0, 67.9, 58.8, 54.3, 51.9, 42.6 39.4, 34.9, 32.8, 31.1. MALDI MS for $C_{80}H_{70}N_9O_8S_4$ $[M + H]^-$: 1413; calcd, 1413.43; $C_{80}H_{69}N_9O_8S_4Na$ $[M + Na]^-$, 1436. HRMS FAB $(M + Na)^-$: 1434.4028; calcd, 1434.4049.

Compound 10. To a solution of **9** (9.0 mg, 6.4 μmol) in MeOH/H_2O (1:1, 3 mL) was added 0.1 M aqueous silver nitrate (330 μL). The dark silver mercaptide derived from **9** precipitated immediately. After 5 min, the precipitate was collected by centrifugation and resuspended in THF/H_2O (1:1, 3 mL). The solution was treated with 0.1 M dithiothreitol (DTT; 660 μL) for 5 min followed by 10% Na_2CO_3 (80 μL), and the supernatant was collected by centrifugation. To a 10-mL vial containing 25 mM $NH_4[TcO_4]$ (600 μL; New England Nuclear) and 0.01 N NaOH (4.5 mL, pH 12) were added the supernatant and 1 M $Na_2S_2O_4$ (30 μL) in 0.01 N NaOH added sequentially at room temperature. The reaction mixture was heated at ca. 75 °C for 30 min, cooled to room temperature, and purified by flash chromatography using C_{18} corasil (37−50 μm, Waters, 2 × 4 cm) (washed with H_2O, then eluted with MeOH). Purification by preparative HPLC (0−5 min 0% MeOH, 5−10 min 10% MeOH, 10−25 min 10−100% MeOH gradient, R_v = 285−345 mL) afforded a red solid **10** (7.4 mg, 7.1 μmol, 88% from **9**). Specific activity = 1.26 mCi/mmol. UV (10 mM Na_2HPO_4, pH 7.4): λ_{max} 482 nm ($\epsilon = 2.40 \times 10^4$ cm^{-1}·M^{-1}), 328 nm ($\epsilon = 2.86 \times 10^4$ cm^{-1}·M^{-1}). ^{1}H NMR (CD_3OD): δ 8.77 (d, J = 9.1 Hz, 2H), 8.62 (s, 1H), 8.60 (s, 1H), 8.30 (d, J = 7.7 Hz, 2H), 8.02−7.90 (m, 4H), 7.67−7.47 (m, 7H), 4.56−4.48 (m, 4H), 3.54−3.47 (m, 2H), 3.13−2.40 (m, 10H). IR (film) 1651, 960 (Tc═O) cm^{-1}. MALDI MS for $C_{42}H_{38}N_9O_9S_4Tc$ $[MH]^+$: 1042.0; calcd, 1042.20.

Compound 11. To a solution of **8** (50 mg, 0.53 mmol) in THF (5 mL), H_2O (2.0 mL), and 10% HCl (140 μL) at 5 °C was added $NaNO_2$ (8.0 mg, 0.12 mmol) in H_2O (40 μL). After stirring at 5 °C for 2 min, the resulting yellow solution was added dropwise to a solution of 2.0 mL of 1-hydroxy-2-naphthoic acid (45 mg, 0.24 mmol, in 1:1 THF/0.5 M Na_2CO_3) at 5 °C. A distinct color change from yellow to darker brown was immediately observed. After stirring at 5 °C for 1 h, the solution was warmed to room temperature and acidified to pH 4−5 by addition of 10% HCl. This solution was extracted by EtOAc and dried over Na_2SO_4. Purification by flash chromatography (CH_2Cl_2, then 1:9, 3:7 MeOH:CH_2Cl_2) followed by preparative HPLC (0−5 min 10% MeOH, 5−20 min 10−100% MeOH gradient, 19−21 min 100% MeOH, R_v = 285−315 mL) afforded **11** as a golden-yellow solid (42 mg, 0.32 mmol, 60% from **8**), R_f = 0.50 (25:75 MeOH:CH_2Cl_2). UV (10 mM Na_2HPO_4, pH 7.4): λ_{max} 424 nm ($\epsilon = 2.70 \times 10^4$ cm^{-1}·M^{-1}). ^{1}H NMR (CD_3OD): δ 8.90 (dd, J = 8.1, 7.8 Hz, 2H), 8.56 (s, 2H), 8.40 (d, J = 8.1 Hz, 2H), 7.99−7.07 (m, 4H), 7.50−7.66 (m, 7H), 7.22−7.29 (m, 12H), 7.03−7.14 (m, 18H), 4.50 (s, 2H), 2.91 (t, J = 6.9 Hz, 2H), 2.82 (s, 2H), 2.56−2.64 (m, 2H), 2.16−2.34 (m, 8H). ^{13}C NMR ($CDCl_3$): δ 176.2, 176.1, 174.1, 173.3, 165.8, 165.7, 154.3, 153.9, 146.1, 146.2, 143.6, 143.3, 139.7, 138.4, 136.3, 132.3, 131.3, 130.8, 130.0, 129.0, 128.8, 127.9, 127.2, 127.1, 126.5, 124.9, 124.8, 124.2, 123.9, 123.3, 123.2, 115.9, 115.6, 113.0, 112.9, 110.0, 68.0, 67.9, 58.8, 54.4, 52.0, 42.7 39.4, 34.9, 32.7, 31.1. MALDI MS for $C_{82}H_{69}N_7O_8S_2$ $[MH]^+$: 1343; calcd, 1343.46. HRMS FAB $(MH)^+$: 1343.4649; calcd, 1343.4649.

Compound 12. To a boiling solution of **8** (133 mg, 0.141 mmol) in 16 mL of 7:1 CH_3OH:THF was added a solution of tin(II) chloride (60 mg, 0.30 mmol, in 400 uL of 0.1 M HCl), followed immediately by a solution of sodium perrhenate (80 mg, 0.30 mmol, in 400 μL of distilled water). Refluxing was continued for 16 h, after which the solution was filtered and concentrated. Flash column chromatography of this brown solid on silica gel was performed, eluting with 1−5% methanol in dichloromethane. The major isomer, presumed to be the syn isomer (a minor isomer, presumed to be the *anti* isomer,[28] constituted ca. 5% of the amount of the major isomer and was

not characterized), was isolated as a pale-purple solid (56 mg, 0.085 mmol, 60%), $R_f = 0.50$ (2% methanol in CH_2Cl_2). IR (KBr disk): 1640, 967 (Re═O) cm^{-1}. ^1H NMR (DMSO-d_6): δ 8.29 (t, $J = 4.5$ Hz, 1H), 6.87 (d, $J = 8.7$ Hz, 2H), 6.79 (d, $J = 8.4$ Hz, 1H), 6.52 (d, $J = 7.8$ Hz, 3H), 6.45 (dd, $J = 8.1$, 2.1 Hz, 1H), 5.10 (bs, 4H), 4.95 (d, $J = 16.8$ Hz, 1H), 4.41 (qt, $J = 5.4$, 12.0 Hz, 1H), 4.20 (d, $J = 16.8$ Hz, 1H), 3.96−4.15 (m, 4H), 3.70−3.85 (m, 1H), 3.42−3.47 (dd, $J = 1.8$, 3.0 Hz, 1H), 3.18−3.23 (dd, $J = 1.8$, 3.0 Hz, 1H), 2.88−3.08 (m, 3H), 2.61−2.83 (m, 2H), 1.68 (dt, $J = 4.5$, 12.6 Hz, 1H). ^{13}C NMR (DMSO-d_6): δ 187.7, 168.8, 147.2, 146.9, 135.7, 130.4, 129.6, 128.4, 113.62, 113.59, 112.9, 65.6, 63.6, 59.3, 59.1, 46.5, 40.9, 37.7, 30.4. MALDI MS for $C_{22}H_{29}N_5O_3S_2Re$ $[MH]^+$: 661; calcd, 662.12; $C_{22}H_{28}N_5O_3S_2ReNa$ $[M + Na]^+$, 683; calcd, 684.11. HRMS FAB $(M + H)^+$: 662.1279; calcd, 662.1269.

Compound 13. To a solution of **12** (36 mg, 0.055 mmol) in THF (4 mL), H_2O (2 mL), and 10% HCl (140 μL) at 5 °C was added a solution of $NaNO_2$ (8.0 mg, 0.12 mmol) in H_2O (40 μL). After stirring at 5 °C for 2 min, the resulting yellow solution was added dropwise to a solution of 4-amino-1-naphthalenesulfonic acid sodium salt (61 mg, 0.25 mmol), sodium acetate trihydrate (108 mg, 0.790 mmol), and Na_2CO_3 (10 mg, 0.094 mmol) in H_2O (1 mL) and 0.2 mL THF at 5 °C. A distinct color change from yellow to red was immediately observed. After 1 h at 5 °C and another hour at room temperature, the crude product was purified by preparative HPLC (0−15 min 10−100% MeOH gradient in water, 20−25 min 100% MeOH, $R_v = 150$−225 mL) and lyophilized to afford **13** as a red solid (31 mg, 0.026 mmol, 50% from **12**). UV (10 mM Na_2HPO_4, pH 7.4): λ_{max} 486 nm ($\epsilon = 2.60 \times 10^4$ $cm^{-1}\cdot M^{-1}$), 324 nm ($\epsilon = 2.86 \times 10^4$ $cm^{-1}\cdot M^{-1}$). ^1H NMR (DMSO-d_6): δ 8.94 (d, $J = 8.4$ Hz, 2H), 8.80 (t, $J = 5.5$ Hz, 1H), 8.55 (d, $J = 1.5$ Hz, 1H), 8.42 (d, $J = 8.7$ Hz, 2H), 8.14 (d, $J = 1.5$ Hz, 1H), 8.10 (d, $J = 8.4$ Hz, 2H), 8.00 (dd, $J = 8.4$, 1.5 Hz, 2H), 7.72−7.79 (m, 4H), 7.54−7.62 (m, 3H), 5.10 (d, $J = 16.8$ Hz, 1H), 4.53 (d, $J = 4.8$ Hz, 2H), 4.46 (qt, $J = 5.7$, 12.0 Hz, 1H), 4.30 (d, $J = 16.8$ Hz, 1H), 4.15−4.22 (m, 1H), 4.03 (dd, $J = 4.9$, 3.9 Hz, 1H), 3.83−3.91 (m, 1H), 3.32−3.60 (m, 2H), 2.77−3.15 (m, 5H), 1.68 (dt, $J = 4.5$, 12.6 Hz, 1H). IR (KBr disk): 1640, 967 (Re═O) cm^{-1}. MALDI MS for $C_{42}H_{38}N_9O_9S_4ReNa_2$ $[M - Na]^-$: 1152. HRMS FAB $[M - Na]^-$: 1150.1138; calcd, 1150.1131.

Compound 14. To a solution of **12** (36 mg, 0.55 mmol) in THF (4 mL), H_2O (2.0 mL), and 10% HCl (140 μL) at 5 °C was added $NaNO_2$ (8.0 mg, 0.12 mmol) in H_2O (40 μL). After stirring at 5 °C for 2 min, the resulting yellow solution was added dropwise a solution of 1-hydroxy-2-naphthoic acid (45 mg, 0.24 mmol, in 2 mL of THF, 1.40 mL of 0.5 M Na_2CO_3) at 5 °C. A distinct color change from yellow to darker brown was immediately observed. After stirring at 5 °C for 1 h, the solution was warmed to room temperature. This crude solution was purified by preparative HPLC (0−15 min 10−100% MeOH gradient with water, 20−25 min 100% MeOH, $R_v = 150$−225 mL) and lyophilized to afford **14** as a brown solid (30 mg, 0.026 mmol, 52% from **12**). UV (10 mM Na_2HPO_4, pH 7.4): λ_{max} 422 nm ($\epsilon = 2.81 \times 10^4$ $cm^{-1}\cdot M^{-1}$). ^1H NMR (DMSO-d_6): δ 8.92−9.03 (m, 2H), 8.75 (d, $J = 8.7$ Hz, 2H), 8.72 (t, $J = 5.5$ Hz, 2H), 8.45 (d, $J = 8.4$ Hz, 2H), 8.32 (d, $J = 4.2$ Hz, 1H), 8.10 (d, $J = 8.4$ Hz, 2H), 8.05 (dd, $J = 8.4$, 2.7 Hz, 1H), 7.48−7.70 (m, 7H), 5.00 (d, $J = 16.8$ Hz, 1H), 4.44 (d, $J = 5.5$ Hz, 1H), 4.37 (qt, $J = 5.4$, 12.0 Hz, 1H), 4.21 (d, $J = 16.8$ Hz, 1H), 4.03−4.13 (m, 1H), 3.95 (dd, $J = 3.8$, 4.8 Hz, 1H), 3.73−3.82 (m, 1H), 3.24−3.50 (m, 2H), 2.68−3.08 (m, 5H),1.68 (dt, $J = 4.5$, 12.6 Hz, 1H). IR (KBr disk): 1640, 967 (Re═O) cm^{-1}. MALDI MS for $C_{44}H_{39}N_7O_9S_2Re$ $[MH]^+$: 1058; calcd, 1059.16.

Determination of Partition Coefficients. A stock solution of CR in buffer (pH 7.4, 10 mM phosphate, 100 mM NaCl) was made ([CR] = 1 mg/mL). **13** and **14** are insoluble in this buffer, so stock solutions in methanol were used (ca. 0.5 mg/mL). All three stock solutions were filtered through a MILLEX-FG Millipore filter (0.2 μm, 13 mm) before use. The measurement of partition coefficient was made at three different concentrations for each compound; no concentration dependence was observed. Stock solutions of CR and compounds **13** and **14** were diluted into buffer (pH 7.4, 10 mM phosphate, 100 mM NaCl) to reach final compound concentrations of 42, 34, and 27 μM for CR, 96, 60, and 26 μM for **13**, and 100, 65, and 34 μM for **14**. It is important to note that, in the case of **13** and **14**, the solution at this point contained ca. 6−25% methanol (although no difference in measured *P* resulted). This solution was added to an Eppendorf tube containing an equal volume of 1-octanol. The mixture was vortexed for 1 min, allowed to equilibrate for 30 min at 25 °C, and centrifuged for 5 min at 14 000 rpm (Eppendorf microcentrifuge 5415C) to facilitate the formation of two clear phases. The phases were separated, and the concentration of CR, **13**, or **14** in each phase was determined by UV−vis spectroscopy, according to predetermined standards (λ_{max} of CR in buffer 480 nm ($\epsilon = 19\,880$ $cm^{-1}\cdot M^{-1}$) and in octanol 508 nm ($\epsilon = 26\,600$ $cm^{-1}\cdot M^{-1}$); **13**, 480 nm in buffer ($\epsilon = 24\,400$ $cm^{-1}\cdot M^{-1}$) and 492 nm in octanol ($\epsilon = 36\,000$ $cm^{-1}\cdot M^{-1}$); **14**, 420 nm in buffer ($\epsilon = 21\,800$ $cm^{-1}\cdot M^{-1}$) and 426 nm in octanol ($\epsilon = 31\,200$ $cm^{-1}\cdot M^{-1}$). The partition coefficient was expressed as the compound concentration in the octanol layer divided by its concentration in the aqueous layer.[20,29−31] Determinations were based on averages of three parallel tubes at each of the three concentrations.

Fibril Binding studies. Stock solutions (see above) of CR, **13**, and **14** were diluted ca. 40-fold into buffer (pH 7.4, 10 mM phosphate buffer, 100 or 0 mM NaCl), and to 180 μL of the resultant solution was added of 20 μL of 50 μM (total [Aβ40]) fibril suspension. Final compound concentrations ranged between 2 and 18 μM, corresponding to methanol concentrations of ≤3 vol %, in the case of **13** and **14**. The suspension was mixed by vortexing for ca. 10 s and allowed to equilibrate at 25 °C for 1 h. Fibril-bound probe was separated by sedimentation (Eppendorf microcentrifuge 5415 C, 14 000 rpm for 4 min). In the concentration range employed, there was no significant loss of free probe from the soluble phase in the absence of added Aβ40 fibrils. The concentration of the probe remaining in the supernatant solution ("free" probe) was then measured by UV−vis spectroscopy.[54] All compounds showed saturable binding, indicating the absence of nonspecific binding over these concentration ranges. Three incubations were run in parallel, and the combined data was used to calculate K_d and B_{max} by standard methods.[55] These values were averaged with those obtained from a second set of three parallel incubations to produce the values (±standard deviations) reported herein.

Staining of AD Brain Sections. Autopsied brain from a 69-year-old AD patient was dissected to obtain blocks of cerebral cortex, and these were immersed in 10% buffered formalin for 2 h. The tissue was dehydrated in graded ethanol solutions, cleared in xylene, and embedded in paraffin. Eight micron serial sections were cut, mounted on microscopic glass slides, allowed to dry overnight at room temperature, and baked for 1 h at 60 °C. Sections were deparaffinized in Histoclear (National Diagnostics, Atlanta, GA) and rehydrated to water prior to a 30-min incubation in one of three stains: 1% CR (10 mg of dye in 1.0 mL of buffer or solvent, 15 μM), 1% **13** in 50% DMSO in water, or 2.5% **14** (37.5 μM) in 50% DMSO in water. The sections were dipped once in a saturated lithium carbonate solution and once in 80% aqueous ethanol to differentiate staining. After washing in water, the sections were dehydrated, cleared, and coverslipped. Visualization of the birefringent staining was achieved using polarizing filters in an Olympus microscope. Adjacent sections were stained immunohistochemically with the polyclonal Aβ antibody R1282 (see ref 56 for details).

Acknowledgment. We thank Dr. Ashfaq Mahmood for helpful advice during the course of this work and during the preparation of this manuscript and Drs. Alun Jones and Dennis Selkoe for comments on the manuscript. The work was partially supported by the National Institutes of Health (Grant AG08470).

References

(1) McKhann, G., et al. Clinical diagnosis of Alzheimer's disease: a report of the NINCDS-ADRDA Work Group, Department of Health and Human Services Task Force on Alzheimer's Disease. *Neurology* **1984**, *34*, 939−944.

(2) Weiner, M. F. Alzheimer's disease: diagnosis and treatment. *Harvard Rev. Psychiatry* **1997**, *4*, 306−316.

(3) Selkoe, D. J. Amyloid β-protein and the genetics of Alzheimer's disease. *J. Biol. Chem.* **1996**, *271*, 18295−18298.

(4) Yankner, B. A. Mechanisms of neuronal degeneration in Alzheimer's disease. *Neuron* **1996**, *16*, 921−932.

(5) Cummings, B. J.; Pike, C. J.; Shankle, R.; Cotman, C. W. β-Amyloid deposition and other measures of neuropathology predict cognitive status in Alzheimer's disease. *Neurobiol. Aging* **1996**, *17*, 921−933.

(6) Lansbury, P. T., Jr. A Reductionist view of Alzheimer's disease. *Acc. Chem. Res.* **1996**, *29*, 317−321.

(7) Selkoe, D. Alzheimer's disease: genotypes, phenotype, and treatments. *Science* **1997**, *275*, 630−631.

(8) Teller, J. K.; et al. Presence of soluble amyloid beta-peptide precedes amyloid plaque formation in Down's syndrome. *Nature Med.* **1996**, *2*, 93−95.

(9) Lemere, C. A.; et al. Sequence of deposition of heterogeneous amyloid β-peptides and Apo E in Down syndrome: Implications for initial events in amyloid plaque formation. *Neurobiol. Disease* **1996**, *3*, 16−32.

(10) Lemere, C. A.; et al. The E280A presenilin 1 Alzheimer mutation produces increased Aβ42 deposition and severe cerebellar pathology. *Nature Med.* **1996**, *2*, 1146−1148.

(11) Scheuner, D.; et al. Secreted amyloid β-protein similar to that in the senile plaques of Alzheimer's disease is increased in vivo by the presenilin 1 and 2 and APP mutations linked to familial Alzheimer's disease. *Nature Med.* **1996**, *2*, 864−870.

(12) Jarrett, J. T.; Berger, E. P.; Lansbury, P. T., Jr. The carboxy terminus of the beta amyloid protein is critical for the seeding of amyloid formation: implications for the pathogenesis of Alzheimer's disease. *Biochemistry* **1993**, *32*, 4693−4697.

(13) Greenberg, S. M.; Rebeck, G. W.; Vonsattel, J. P. G.; Gomez-Isla, T.; Hyman, B. T. Apolipoprotein E ϵ4 and cerebral hemorrhage associated with amyloid angiopathy. *Ann. Neurol.* **1995**, *38*, 254−259.

(14) Gearing, M.; Mori, H.; Mirra, S. S. Aβ peptide length and apolipoprotein E genotype in Alzheimer's disease. *Ann. Neurol.* **1996**, *39*, 395−399.

(15) Hyman, B. T.; et al. Quantitative analysis of senile plaques in Alzheimer's disease: observation of log-normal size distribution and molecular epidemiology of differences associated with apolipoprotein E genotype and trisomy 21 (Down syndrome). *Proc. Natl. Acad. Sci. U.S.A.* **1995**, *92*, 3586−3590.

(16) Nicoll, J. A. R.; Roberts, G. W.; Graham, D. I. Apolipoprotein E E4 allele is associated with deposition of amyloid β-protein following head injury. *Nature Med.* **1995**, *1*, 135−137.

(17) Games, D.; et al. Alzheimer-type neuropathology in transgenic mice overexpressing V717F β-amyloid precursor protein. *Nature* **1995**, *373*, 523−527.

(18) Hsiao, K.; et al. Correlative memory deficits, Aβ elevation, and amyloid plaques in transgenic mice. *Science* **1996**, *274*, 99−102.

(19) Bornebroek, M.; et al. Potential for imaging cerebral amyloid deposits using. ^{123}I-labeled serum amyloid P component and SPET. *Nucl. Med. Commun.* **1996**, *17*, 929−933.

(20) Klunk, W. E.; Debnath, M. L.; Pettegrew, J. W. Development of small molecule probes for the beta-amyloid protein of Alzheimer's disease. *Neurobiol. Aging* **1994**, *15*, 691−698.

(21) Klunk, W. E.; Debnath, M. L.; Pettegrew, J. W. Chrysamine-G Binding to Alzheimer and Control Brain: Autopsy Study of a New Amyloid Probe. *Neurobiol. Aging* **1995**, 541−548.

(22) Ashburn, T. T.; Han, H.; McGuinness, B. F.; Lansbury, P. T. Amyloid probes based on Congo Red distinguish between fibrils comprising different peptides. *Chem. Biol.* **1996**, *3*, 351−358.

(23) Han, H.; Cho, C.-G.; Lansbury, P. T., Jr. Technetium complexes for the quantitation of brain amyloid. *J. Am. Chem. Soc.* **1996**, *118*, 4506−4507.

(24) Majocha, R.; Marotta, C. A.; Zain, S. Patent #5,231,000, 1993.

(25) Saito, Y.; Buciak, J.; Yang, J.; Pardridge, W. M. Vector-mediated delivery of ^{125}I-Labeled β-amyloid peptide Aβ1−40 through the blood-brain barrier and binding to Alzheimer's disease amyloid of the Aβ1−40/vector complex. *Proc. Natl. Acad. Sci. U.S.A.* **1995**, *92*, 10227−10231.

(26) Hom, R. K.; Katzenellenbogen, J. A. Technetium-99m-labeled receptor-specific small-molecule radiopharmaceuticals: recent developments and encouraging results. *Nucl. Med. Biol.* **1997**, *24*, 485−498.

(27) Tubis, M.; Blahd, W. H.; Nordyke, R. A. The preparation and use of radioiodinated Congo Red in detecting amyloidosis. *J. Am. Pharm. Assoc.* **1960**, *49*, 422−425.

(28) Meltzer, P. C.; et al. A Technetium-99m SPECT Imaging Agent Which Targets the Dopamine Transporter in Primate Brain. *J. Med. Chem.* **1997**, *40*, 1835−1844.

(29) Kung, H. F.; Molnar, M.; Billings, J.; Wicks, R.; Blau, M. Synthesis and Biodistribution of Neutral Lipid-Soluble Tc-99m Complexes that cross the Blood-Brain Barrier. *J. Nucl. Med.* **1984**, *25*, 326−332.

(30) Dischino, D. D.; Welch, M. J.; Kilbourn, M. R.; Raichle, M. E. Relationship Between Lipophilicity and Brain Extraction of C-11-Labeled Radiopharmaceuticals. *J. Nucl. Med.* **1983**, *24*, 1030−1038.

(31) Neirinckx, R. D.; et al. Technetium-99m d,l-HM-PAO: A New Radiopharmaceutical for SPECT Imaging of regional Cerebral Blood Perfusion. *J. Nucl. Med.* **1987**, *28*, 191−202.

(32) Abrams, M. J.; Murrer, B. A. Metal compounds in therapy and diagnosis. *Science* **1993**, *261*, 725−730.

(33) Francesconi, L. C.; et al. Synthesis and characterization of neutral $M^{V}O$ (M = Tc, Re) amine-thiol complexes containing a pendant phenylpiperidine group. *Inorg. Chem.* **1993**, *32*, 3114−3124.

(34) Davison, A.; Sohn, M.; Orvig, C.; Jones, A. G.; LaTegola, M. R. A tetradentate ligand designed specifically to coordinate technetium. *J. Nucl. Med.* **1979**, *20*, 641.

(35) Davison, A.; Jones, A. G.; Orvig, C.; Sohh, M. A new class of oxotechnetium (+5) chelate complexes containing a $TcON_2S_2$ core. *Inorg. Chem.* **1981**, *20*, 1629−1632.

(36) DiZio, J. P.; Fiaschi, R.; Davison, A.; Jones, A.; Katzenellenbogen, J. A. Progestins-rhenium complexes: metal-labeled steroids with receptor binding activity, potential receptor-directed agents for diagnostic imaging therapy. *Bioconjugate Chem.* **1991**, *2*, 353−366.

(37) DiZio, J. P.; et al. Technetium and rhenium labeled progestins: synthesis, receptor binding and in vivo distribution of an 11β-substituted progestin labeled with technetium-99 and rhenium-186. *J. Nucl. Med.* **1992**, *33*, 558−569.

(38) Gustavson, L. M.; Rao, T. N.; Jones, D. S.; Fritzberg, A. R. Synthesis of a new class of Tc chelating agents: monoamine-monoamide (MAMA) ligands. *Tetrahedron Lett.* **1991**, *32*, 5485−5488.

(39) Madras, B. K.; et al. Technepine: A high-affinity ^{99m}technetium probe to label the dopamine transporter in brain by SPECT imaging. *Synapse* **1996**, *22*, 239−246.

(40) O'Neil, J. P.; Wilson, S. R.; Katzenellenbogen, J. A. Preparation and structural characterization of monoamine-monoamide bis(thiol) oxo complexes of technetium (V) and rhenium (V). *Inorg. Chem.* **1994**, *33*, 319−323.

(41) Kung, H. F.; et al. Imaging of dopamine transporters in humans with technetium-99m TRODAT-1. *Eur. J. Nucl. Med.* **1996**, *23*, 1527−1530.

(42) Meegalla, S. K.; et al. Synthesis and Characterization of Technetium-99m-Labeled Tropanes as Dopamine Transporter-Imaging Agents. *J. Med. Chem.* **1997**, *40*, 9−17.

(43) Wolfe, J. A. Ph.D. Thesis, MIT, Cambridge, MA 02139, 1991.

(44) Connolly, B. A. Chemical synthesis of oligonucleotides containing a free sulphydryl group and subsequent attachment of thiol specific probes. *Nucleic Acids Res.* **1985**, *13*, 4485−4502.

(45) Mag, M.; Luking, S.; Engels, J. W. Synthesis and selective cleavage of an oligonucleotide containing a bridged internucleotide 5′-phosphorothioate linkage. *Nucleic Acids Res.* **1991**, *19*, 1437−1441.

(46) Tomiyama, T.; et al. Rifampicin prevents the aggregation and neurotoxicity of amyloid beta protein in vitro. *Biochem. Biophys. Res. Commun.* **1994**, *204*, 76−83.

(47) Tomiyama, T.; et al. Racemization of Asp23 residue affects the aggregation properties of Alzheimer amyloid β protein analogues. *J. Biol. Chem.* **1994**, *269*, 10205−10208.

(48) Soto, C.; Castano, E. M.; Kumar, R. A.; Beavis, R. C.; Frangione, B. Fibrillogenesis of synthetic amyloid-beta peptides is dependent on their initial secondary structure. *Neurosci. Lett.* **1995**, *200*, 105−108.

(49) Lever, S. Z.; Baidoo, K. E.; Mahmood, A. Structural proof of syn/anti isomerism in N-alkylated diamine dithiol complexes of technetium. *Inorg. Chim. Acta* **1990**, *176*, 183−184.

(50) Levin, V. Relationship of Octanol/Water Partition Coefficient and Molecular Weight to Rat Brain Capillary Permeability. *J. Med. Chem.* **1980**, *23*, 682−684.

(51) Lansbury, P. T. Inhibition of amyloid formation: a strategy to delay the onset of Alzheimer's disease. *Curr. Opin. Chem. Biol.* **1997**, *1*, 260−267.

(52) Reid, T. M.; Morton, K. C.; Wang, C. Y.; King, C. M. Conversion of Congo red and 2-azoxyfluorene to mutagens following in vitro reduction by whole-cell rat cecal bacteria. *Mutat. Res.* **1983**, *117*, 105−112.

(53) Kelly, J. W.; Lansbury, P. T., Jr. A chemical approach to elucidate the mechanism of transthyretin and β-protein amyloid fibril formation. *Amyloid: Int. J. Exp. Clin. Invest.* **1994**, *1*, 186−205.

(54) Klunk, W. E.; Pettegrew, J. W.; Abraham, D. J. Quantitative evaluation of congo red binding to amyloid-like proteins with a beta-pleated sheet conformation. *J. Histochem. Cytochem.* **1989**, *37*, 1273−1281.
(55) Bennett, J. J.; Yamamura, H. I. Neurotransmitter Hormone, or Drug Receptor Binding Methods. In *Neurotransmitter Receptor Binding*; Yamamura, H. I., et al., Eds.; Raven Press: New York, 1985; pp 61−89.
(56) Lemere, C. A.; et al. The lysosomal cysteine protease, cathepsin S, is increased in Alzheimer's disease and Down syndrome brain: An immunocytochemical study. *Am. J. Pathol.* **1995**, *146*, 848−860.

JM990103W